Hafnium boosts charge carrier dynamics in hematite for improved

solar water splitting

Gustavo M. Morishita^{a, b}, Ingrid Rodríguez-Gutiérrez^{a, b}, Ricardo H. R. Castro^d, Flavio L.

Souza^{a, b,c*}

^aFederal University of ABC (UFABC), Av. dos Estados Nº 5001, Bangu, Santo André, São

Paulo, CEP 09210-580, Brazil

^bBrazilian National Nanotechnology Laboratory (LNNANO), Brazilian Center for Research in

Energy and Materials (CNPEM), Campinas, São Paulo CEP 13083-100, Brazil

^cInstitute of Chemistry, University of Campinas (UNICAMP), PO Box 6154, Campinas, São

Paulo 13083-970, Brazil

^dUniversity of California, Davis, Department of Materials Science and Engineering, One

Shields Ave, Davis, CA 95616, USA.

* Corresponding author: flavio.souza@lnnano.cnpem.br

Abstract

The work demonstrates a three-fold increase in the photoelectrochemical efficiency of hematite

nanorods due to the combination of Hafnium doping and the incorporation of a ZrO₂ underlayer

on FTO. While the ZrO2 layer reduced the electron loss from the back-injection into the FTO

contact support, Hafnium doping did not significantly alter the hematite lattice structure. But

rather, Hafnium induced nanorod diameter reduction from 32±2 and 26±2 nm, with a

consequent increase in the active surface area. The linear sweep voltammetry measurements

with 100 mW cm⁻² illumination in a 500 nm photoanode thickness showed a photocurrent

density of 2.07 mA cm⁻² at 1.23 V in a reversible hydrogen electrode (RHE). The value contrasts

with the bare hematite rods (0.75 mA cm⁻²), highlighting the photoanode design's role in

improving solar power hydrogen production.

Keywords: hematite nanorods, solar energy conversion, charge carrier dynamics, doping

1. Introduction

Hematite (α -Fe₂O₃) is a potential photoanode for photoelectrochemical (PEC) water splitting to produce green hydrogen. However, its conversion efficiency is still far below practical values due to inherent challenges, such as sluggish surface oxygen evolution reaction, rapid electron-hole recombination, and limited conductivity [1,2]. Several strategies have been employed to overcome the limitations, including nanostructuring, crystal doping, and interfacial segregation [3–6]. From these strategies, increasing the number of active sites and enhancing electron transport through morphology control is a suitable path accomplishable by a controlled synthesis. In particular, 1D nanostructures have shown PEC responses much superior to planar structures, with a benchmark photocurrent of \sim 6 mA cm⁻² achieved for nanorods using combined modifications of hydrogen treatment, TiO₂ overlayer, and cobalt phosphate catalysts [6].

Due to the performance limitations of the hematite potential, tetravalent ions, such as Ti⁴⁺, Zr⁴⁺, Sn⁴⁺, and Si⁴⁺, have been proposed to improve charge carrier mobility [3,7]. Because the intrinsic mobility and carrier concentration are impacted by surface polarons [8], favoring doping segregation in contrast to solid solutions by synthetic strategies causes a shift in photocurrent onset potential to positive values [5], indicating modification of the charge carrier kinetics.

This work investigates the underexplored Hf⁴⁺-doping effects on the charge carrier dynamics in hematite nanorods arrays, and their respective performance as photoanodes. In addition to Hf⁴⁺, we introduced a ZrO₂ layer at the transparent conducting oxide/Hf-hematite interface to minimize electron losses at back-contact injection from the FTO surface, altogether resulting in an overall three-fold increase in photoelectrochemical efficiency.

2. Experimental Section

Rod-like hematite was obtained by thermally converting a β-FeOOH film prepared on a FTO substrate by immersing it into an iron precursor solution followed by hydrothermal treatment [9]. The ZrO₂ underlayer was introduced by previously spin-coating a Zr-salt solution onto the FTO. Hf⁴⁺ was deposited over β-FeOOH before the conversion to hematite. Pristine hematite is labeled as H, Hf-doped as HHf, and that containing the underlayer as Zr/HHf. Details of the synthesis and PEC testing conditions are found in Supplemental Informations.

3. Results and discussions

The X-ray diffraction patterns confirmed the formation of the hematite (α -Fe₂O₃, JCPDS card 033-0664, Fig. S4). Additional diffraction peaks associated with Hf⁴⁺ and ZrO₂ underlayer additions were not detected. Calculated Lotgering factor [10] (f = 0.44, 0.46, and 0.44 for H, HHf, and Zr/HHf, respectively) revealed preferential growth at (110) directions, likely induced by FTO [11]. The crystallite sizes estimated from the Scherrer equation [12] indicate crystal growth suppression by Hf⁴⁺ (32±2 and 26±2 nm for H and HHf, respectively). The result for Zr/HHf (24±2 nm) suggests the ZrO₂ underlayer does not significantly impact the crystallite size. The cell parameters showed a small volume expansion from 301.779 Å³ (H) to 301.869 Å³ (HHf), and to 301.892 Å³ (Zr/HHf). However, these are within the uncertainty of ±0.35, suggesting negligible dissolution of Zr and Hf into the hematite crystal.

Fig. 1 shows images of the photoanodes formed by nanorods with a thickness of 500±30 nm, 502±30 nm, and 537±30 nm, and diameters of 54±11 nm, 31±7 nm, and 30±5 nm for H, HHf, and Zr/HHf, respectively. Consistent with the crystallite sizes, Hf also impacted the rod dimensions. However, the thickness variation in Zr/HHf is related to the addition of ZrO₂ underlayer. For all samples, AFM showed minor variations in the Root Mean Square (RMS) (102±3 nm, 96±6 nm, and 101.7±2 nm for H, HHf, and Zr/HHf respectively), indicating consistent surface roughness.

Insert Figure 1

Fig. 2a shows the linear sweep voltammetry measurements under dark conditions and 100 mW cm⁻² illumination. The photocurrent density (J_{ph}) versus applied potential (in reversible hydrogen electrode – RHE) curves show the photocurrent response at 1.23 V_{RHE} for H, HHf, and Zr/HHf photoanodes are 0.75, 1.80, and 2.07 mA cm⁻², respectively. A slight photocurrent onset shift at more positive potential is observed after Hf addition, associated with the creation of additional surface defects [5]. The experimental photocurrent density (J_{abs}) derived from the absorbance spectrum and calculated from Eq. S1 in Supporting Information (Fig. 2b) present a slightly decrease (8.8±0.2, 7.6±0.1, and 8.0±0.3 mAcm⁻² for H, HHf, and Zr/HHf). More importantly, we observe significant enhancement in overall efficiency (η_{overall}), determined by the ratio between J_{ph} and J_{abs}, from 8%±0.5 for H to 22%±3.2, and 26±0.8% for HHf and Zr/HHf.

While Hf⁴⁺ significantly improves the photocurrent to values consistent with the recent literature exploring Hf⁴⁺ incorporation [13], the ZrO₂ underlayer also played an essential role by mitigating electron loss and inhibiting Sn self-doping. The quality of this underlayer was tested by measuring cyclic voltammetry (CV) of FTO and FTO with Zr-underlayer deposited (Fig. S2). A broad peak in 0.9 Erhe was observed, indicating the electron injected from the photoanode was transferred (lost) to the electrolyte before arriving at the counter-electrode. In counterparty, the underlayer linear curve shows electron loss prevention.

Mott-Schottky analysis under dark conditions helped understand the combined Hf and ZrO₂ underlayer effects. Intrinsic properties such as donor density (N_D), flat band potential (V_{fb}), and depletion layer width (W) are shown in Fig. 2c. Both N_D, calculated from Eq. S2, (4.5x10¹⁹, 3.3 x10¹⁹, and 2.8 x10¹⁹ cm³ for H, HHf, and Zr/HHf, respectively) and V_{fb},

determined by Gärtner-Butler approximation with H_2O_2 as hole scavenger (V_{fb} =0.6 for all photoanodes) [14], remained constant. W, obtained from Eq. S3, varied slightly (17, 21, and 22 nm for H, HHf, and Zr/HHf, respectively). Combined, the data indicate that neither Hf nor ZrO₂ significantly change the hematite electronic properties but are mainly modifying its charge carrier kinetics.

Insert Figure 2

Intensity modulate photocurrent spectroscopy (IMPS) was used to investigate the charge carrier dynamic, by analyzing the external quantum efficiency (*EQE*), charge separation efficiency (*CSE*), surface recombination (*ksr*) and transfer (*ktr*) constants as a function of the applied potential. From Nyquist plot, the IMPS transfer function for H (Fig. S3a) is composed of a high-frequency and low-frequency loop in all potential ranges, the latter associated with the charge recombination due to the presence of surface states. For HHf (Fig. S3 b), the loop disappears at V_{RHE}>1.3 V_{RHE}. For Zr/HHf (Fig. 2d), the loop disappears at V_{RHE}>1.2 V_{RHE}, indicating that the surface processes no longer depend on the applied potential.

Similar trends for all photoanodes are seen in the k_{tr} deconvoluted from the IMPS spectra (Fig. 2e), indicating the transfer constant is unaltered by Hf or ZrO₂. Similarly, a constant trend for (RC)⁻¹ time is observed. However, in Fig. 2f, a more pronounced decrease in k_{sr} for HHf and Zr/HHf photoanodes suggests that Hf⁴⁺ alters the surface processes. Interestingly, the intercept at medium frequency related to CSE is significantly greater for Zr/HHf and HHf than for H, confirming that Hf and ZrO₂ are mainly improving the electron collection, which justifies this enhancement in charge separation.

4. Conclusions

Hf-doping improves the PEC performance by enhancing charge separation efficiency. Introducing the ZrO₂ underlayer helps avoid electron losses at the FTO back contact, improving electron collection, and positively impacting the charge separation. Combined, this rational design offers a strategy to improve the PEC performance of hematite nanorod array photoanodes for solar water splitting.

Declaration of Competing Interest

None.

Acknowledgments

CAPES, CNPQ, and FAPESP (São Paulo Research Foundation, Grants 17/02317-2, 13/07296-2, 17/11986-5 and 22/0410-6), Shell, ANP (Brazil's National Oil, Natural Gas, and Biofuels Agency) through the R&D levy regulation. The authors thank Fabiano Montoro and João M Silva for the SEM. RC thanks NSF DMR2015650.

Supplementary data

The following are the Supplementary data to this article: experimental details, Cyclic Voltammetry, Intensity modulated photocurrents spectroscopy data, and X-ray diffraction patterns.

References

- [1] K. Sivula, Metal oxide photoelectrodes for solar fuel production, surface traps, and catalysis, J. Phys. Chem. Lett. 4 (2013) 1624–1633. https://doi.org/10.1021/jz4002983.
- [2] M.G. Walter, E.L. Warren, J.R. McKone, S.W. Boettcher, Q. Mi, E.A. Santori, N.S. Lewis, Solar water splitting cells, Chem. Rev. 110 (2010) 6446–6473. https://doi.org/10.1021/cr1002326.
- [3] J.B. Souza Junior, F.L. Souza, L. Vayssieres, O.K. Varghese, On the relevance of understanding and controlling the locations of dopants in hematite photoanodes for low-

- cost water splitting, Appl. Phys. Lett. 119 (2021) 200501. https://doi.org/10.1063/5.0066931.
- [4] J. Zhang, J. Cui, S. Eslava, Oxygen evolution catalysts at transition metal oxide photoanodes: their differing roles for solar water Splitting, Adv. Energy Mater. 11 (2021) 2003111. https://doi.org/10.1002/aenm.202003111.
- [5] A.L.M. Freitas, D.N.F. Muche, E.R. Leite, F.L. Souza, Interface engineering of nanoceramic hematite photoelectrode for solar energy conversion, J. Am. Ceram. Soc. 103 (2020) 6833–6846. https://doi.org/10.1111/jace.17390.
- [6] T.H. Jeon, G. Moon, H. Park, W. Choi, Ultra-efficient and durable photoelectrochemical water oxidation using elaborately designed hematite nanorod arrays, Nano Energy. 39 (2017) 211–218. https://doi.org/10.1016/j.nanoen.2017.06.049.
- [7] K. Kang, H. Zhang, J.H. Kim, W.J. Byun, J.S. Lee, An in situ fluorine and ex situ titanium two-step co-doping strategy for efficient solar water splitting by hematite photoanodes, Nanoscale Adv. 4 (2022) 1659–1667. https://doi.org/10.1039/D2NA00029F.
- [8] T.J. Smart, V.U. Baltazar, M. Chen, B. Yao, K. Mayford, F. Bridges, Y. Li, Y. Ping, Doping bottleneck in hematite: multipole clustering by small polarons, Chem. Mater. 33 (2021) 4390–4398. https://doi.org/10.1021/acs.chemmater.1c00304.
- [9] L. Vayssieres, N. Beermann, S.-E. Lindquist, A. Hagfeldt, Controlled aqueous chemical growth of oriented three-dimensional crystalline nanorod arrays: application to iron(III) oxides, Chem. Mater. 13 (2001) 233–235. https://doi.org/10.1021/cm001202x.
- [10] F.K. Lotgering, Topotactical reactions with ferrimagnetic oxides having hexagonal crystal structures I, J. Inorg. Nucl. Chem. 9 (1959) 113–123. https://doi.org/10.1016/0022-1902(59)80070-1.
- [11] M. Cornuz, M. Grätzel, K. Sivula, Preferential orientation in hematite films for solar hydrogen production via water splitting, Chem. Vap. Depos. 16 (2010) 291–295. https://doi.org/10.1002/cvde.201004292.
- [12] G.W. Morey, New crystalline silicates of potassium and sodium, their preparation and general properties., J. Am. Chem. Soc. 36 (1914) 215–230. https://doi.org/10.1021/ja02179a002.
- [13] H. Ma, W. Chen, Q. Fan, C. Ye, M. Zheng, J. Wang, Regulating Sn self-doping and boosting solar water splitting performance of hematite nanorod arrays grown on fluorine-doped tin oxide via low-level Hf doping, J. Colloid Interface Sci. 625 (2022) 585–595.

https://doi.org/10.1016/j.jcis.2022.06.055.

[14] M.A. Butler, Photoelectrolysis and physical properties of the semiconducting electrode WO₂, J. Appl. Phys. 48 (1977) 1914–1920. https://doi.org/10.1063/1.323948.

Fig. 1 a, b, and c show a topographic scan of AFM for H, HHf, and Zr/HHf. a", b", and c" DualBeam images of the lateral view of each sample. a"', b"', and c" shows a topographic views.

Fig. 2 a) Linear Sweep Voltammetry measurement in dark and under one sun irradiation. b) Compilation of the parameters J_{ph}, J_{abs}, and η_{overall}. c) Mott-Schottky in dark condition from Electrochemical Impedance Spectroscopy. d) Intensity-Modulated Photocurrent Spectroscopy spectra with high-intensity blue LED (470 nm) of Zr/HHf. e) Transfer and RC constants versus applied potentials. f) Recombination and RC constants versus applied potentials.

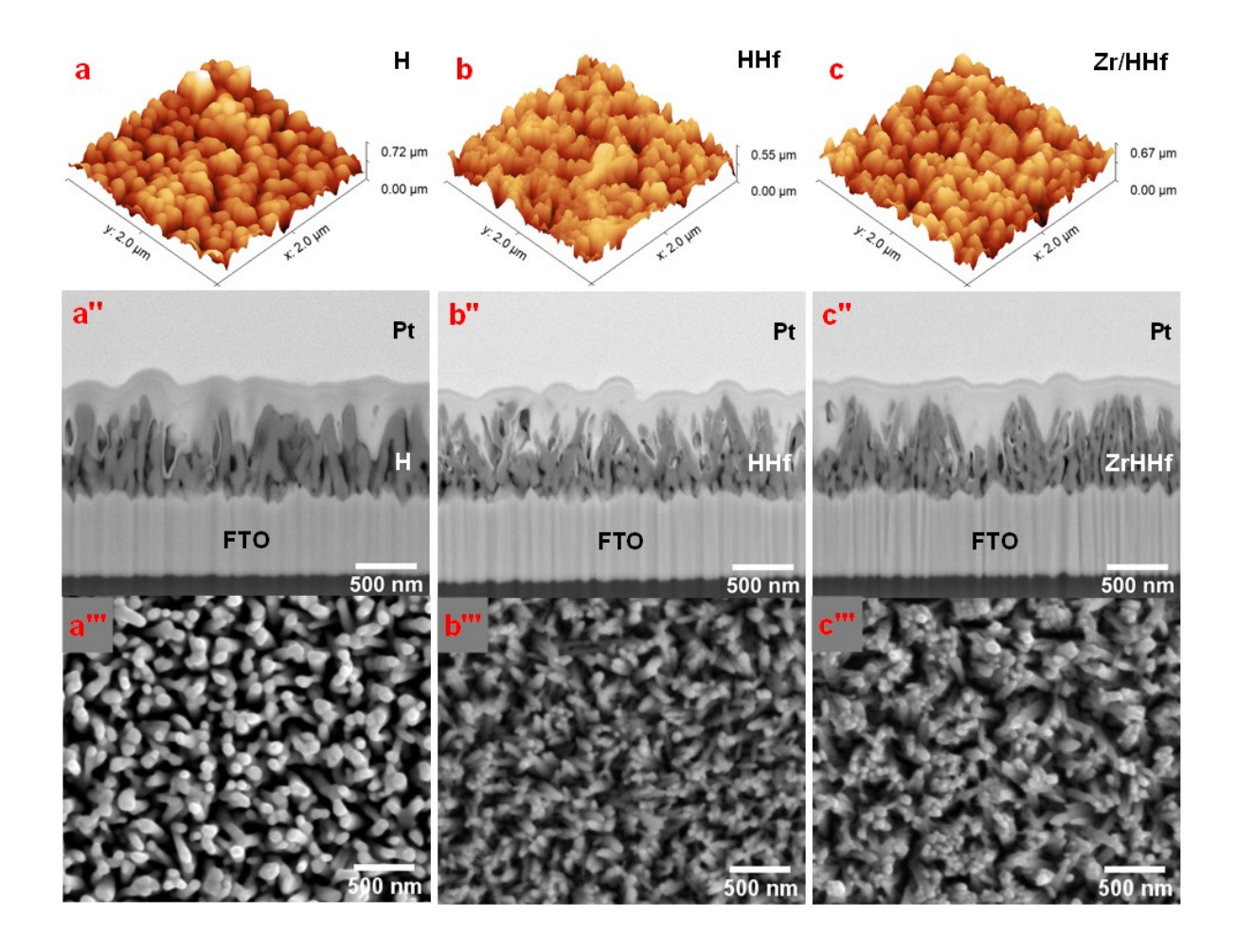


Fig. 1

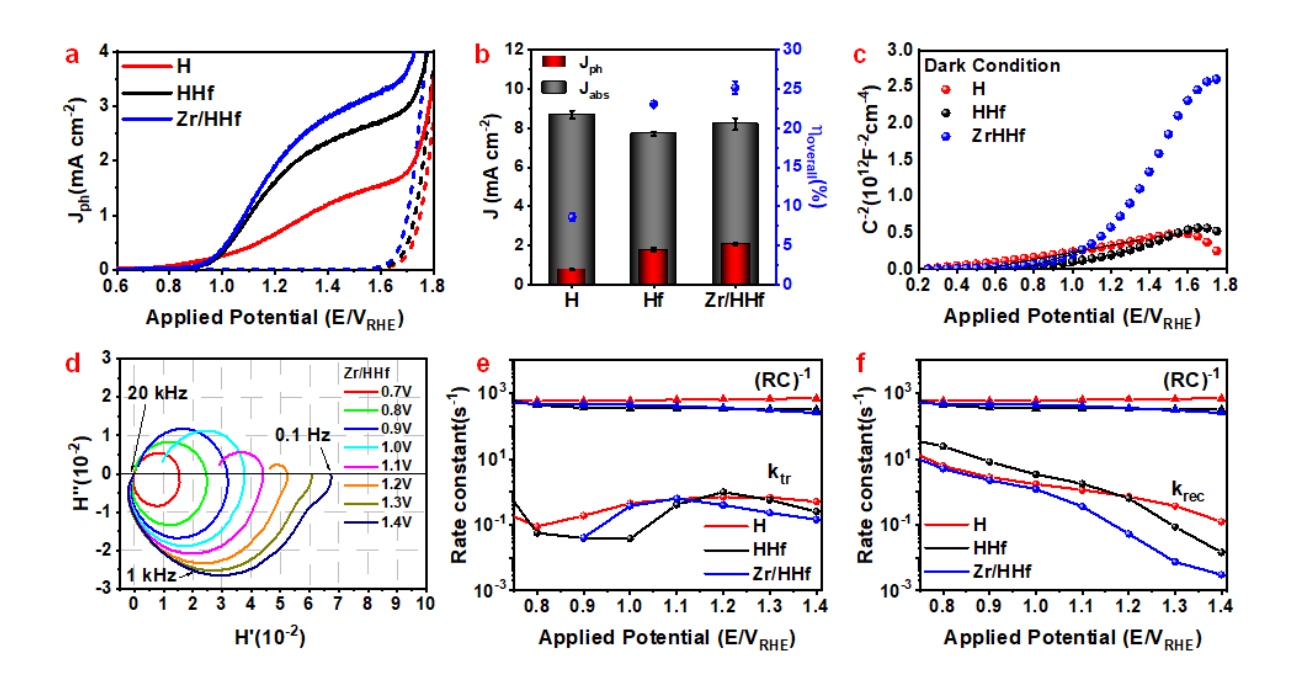


Fig. 2